Tidal origin of NGC 1427A in the Fornax cluster

Lee-Waddell, K.; Serra, P.; Koribalski, B.; Venhola, A.; Iodice, E.; Catinella, B.; Cortese, L.; Peletier, R.; Popping, A.; Keenan, O.

Published in:
Monthly Notices of the Royal Astronomical Society

DOI:
10.1093/mnras/stx2808

Publication date:
2018

Monthly Notices
of the
ROYAL ASTRONOMICAL SOCIETY

MNRAS **474,** 1108–1115 (2018)
Advance Access publication 2017 October 31

doi:10.1093/mnras/stx2808

Tidal origin of NGC 1427A in the Fornax cluster

K. Lee-Waddell,[1⋆] P. Serra,[1,2] B. Koribalski,[1] A. Venhola,[3,4] E. Iodice,[5] B. Catinella,[6] L. Cortese,[6] R. Peletier,[3] A. Popping,[6,7] O. Keenan[8] and M. Capaccioli[9]

[1]*CSIRO Astronomy and Space Sciences, Australia Telescope National Facility, PO Box 76, Epping, NSW 1710, Australia*
[2]*INAF – Osservatorio Astronomico di Cagliari, Via della Scienza 5, I-09047 Selargius (CA), Italy*
[3]*Kapteyn Astronomical Institute, University of Groningen, PO Box 800, NL-9700 AV Groningen, the Netherlands*
[4]*Astronomy Research Unit, University of Oulu, FI-90014 Oulu, Finland*
[5]*INAF – Astronomical Observatory of Capodimonte, via Moiariello 16, Naples I-80131, Italy*
[6]*International Centre for Radio Astronomy Research, The University of Western Australia, 35 Stirling Hwy, Crawley, WA 6009, Australia*
[7]*ARC Centre of Excellence for All-sky Astrophysics (CAASTRO)*
[8]*School of Physics and Astronomy, Cardiff University, Queens Buildings, The Parade, Cardiff CF24 3AA, UK*
[9]*Dip.di Fisica Ettore Pancini, University of Naples 'Federico II', C.U. Monte SantAngelo, Via Cinthia, I-80126 Naples, Italy*

Accepted 2017 October 26. Received 2017 October 15; in original form 2017 March 31

ABSTRACT

We present new HI observations from the Australia Telescope Compact Array and deep optical imaging from OmegaCam on the VLT Survey Telescope of NGC 1427A, an arrow-shaped dwarf irregular galaxy located in the Fornax cluster. The data reveal a star-less HI tail that contains ∼10 per cent of the atomic gas of NGC 1427A as well as extended stellar emission that shed new light on the recent history of this galaxy. Rather than being the result of ram pressure induced star formation, as previously suggested in the literature, the disturbed optical appearance of NGC 1427A has tidal origins. The galaxy itself likely consists of two individual objects in an advanced stage of merging. The HI tail may be made of gas expelled to large radii during the same tidal interaction. It is possible that some of this gas is subject to ram pressure, which would be considered a secondary effect and implies a north-west trajectory of NGC 1427A within the Fornax cluster.

Key words: galaxies: individual: NGC 1427A – galaxies: interactions.

1 INTRODUCTION

Galaxy clusters are often turbulent environments that host various types of galaxies at different stages of evolution (e.g. Mihos et al. 2005; Toloba et al. 2014). Tidal interactions in the outskirts give way to ram pressure stripping in the central regions of clusters (Gunn & Gott 1972; Toomre & Toomre 1972), offering the ability for a side-by-side comparison of these two mechanisms.

In low-density regions, encounters between galaxies can produce extended tidal tails of stars and gas. These tails can constrain the properties of interaction event and be used to investigate the environmental dynamics of a system (e.g. Bournaud et al. 2007). As galaxies move towards the cluster potential, the gas in their outer disc and/or in any of these tidal tails becomes susceptible to ram pressure stripping. The interior region of clusters is typically dominated – in number – by dwarf elliptical galaxies (dEs; Toloba et al. 2014). Many of these dEs started as star-forming irregular galaxies and experienced rapid evolution as the intracluster medium (ICM) depleted their gas content through ram pressure stripping (e.g. Kenney et al. 2014). In this paper, we study the properties of NGC 1427A, a dwarf galaxy evolving near (possibly within) the Fornax cluster.

1.1 The Fornax dwarf NGC 1427A

The Fornax cluster is a compact (virial radius of 0.7 Mpc), low-mass (7×10^{13} $M_\odot$ within a 1.4 Mpc radius) cluster consisting of 108 spectroscopically confirmed galaxies – with magnitudes between $-16 < M_B < -13.5$, a mean velocity of 1493 ± 36 km s^{-1} and a velocity dispersion of 374 ± 26 km s^{-1} – located ∼20 Mpc away (Drinkwater, Gregg & Colless 2001a). Its high central galactic density and low velocity dispersion (Drinkwater et al. 2001b) suggest that tidal interactions could be playing a prominent role in the evolution of cluster members, in addition to ram pressure stripping. NGC 1399 is considered to be the central galaxy of the cluster and located within a projected distance of ∼100 kpc from this centre is NGC 1427A, a bright arrow-shaped dwarf irregular (dIrr).

One of the earliest detailed optical studies of NGC 1427A was conducted by Cellone & Forte (1997) who attributed the distorted shape of this galaxy to tidal forces and suggested that a northern stellar clump might be a separate object that recently interacted with NGC 1427A, causing a burst in star formation. B, V, I and

⋆ E-mail: karen.lee-waddell@csiro.au

Hα imaging by Hilker et al. (1997) revealed that the majority of the brighter OB associations and HII regions in NGC 1427A are aligned along its south-west edge. They identified ∼30 stellar clusters – uniformly distributed over the entire galaxy – which appear to have mean ages less than 2 Gyr, indicating recent starbursts as the result of either an interacting interloper or ram pressure triggered star formation (Hilker et al. 1997). Chaname, Infante & Reisenegger (2000) used long-slit spectroscopy on the seven brightest HII regions across NGC 1427A to show that the aforementioned northern clump has the same velocity pattern as the rest of the galaxy and is likely a part of NGC 1427A (rather than an intruder). With deep optical imaging, Mora, Chaname & Puzia (2015) estimate that the most recent episode of star formation in NGC 1427A began ∼4 Myr ago and that the current star cluster formation rate of this dIrr is consistent with other starburst galaxies. Accordingly, the morphological properties of NGC 1427A were deemed the result of its passage through and interaction with the hot intracluster gas of the cluster (Chaname et al. 2000; Mora et al. 2015).

In this paper, we use new radio and optical observations to investigate whether ram pressure is the primary hydrodynamic interaction that is affecting NGC 1427A. We present arcminute-resolution HI observations – taken with the Australia Telescope Compact Array (ATCA) – and deep optical imaging from OmegaCam on the VLT Survey Telescope (VST) which elucidate the structure of and the evolutionary history for NGC 1427A. In Section 2, we describe the observations of the Fornax cluster with focus on NGC 1427A. Section 3 summarizes the measured results and describes the newly resolved HI tail and key stellar features of NGC 1427A. In Section 4, we compare our data with results and conclusions presented in the literature as well as discuss the possible origin of this tail. We present our final conclusions in Section 5.

2 OBSERVATIONS

There have been numerous surveys of the Fornax cluster (e.g. Bureau, Mould & Staveley-Smith 1996; Drinkwater et al. 2001a; Waugh et al. 2002). Many of these surveys are broadly focused on general detection and cluster properties as a whole. For a more in-depth study of NGC 1427A, we utilized a small portion of the data from two fairly recent high-resolution surveys, as described in this section.

2.1 ATCA HI observations

A blind HI survey of the Fornax cluster was conducted using ATCA's 750B array in late 2013 (project code C2894; PI: P. Serra). A 13 deg^2 field centred on the cluster was observed using multiple pointings over a 28 d period (totalling 331 hr). The fully mosaicked field comprises a hexagonal grid of 756 pointings with 8.7 arcmin spacing (∼2 times better than Nyquist sampling at 1.4 GHz). Each day (i.e. during each ∼12 hr observation), we mosaicked a field of ∼0.7 × 0.7 deg^2 using 27 pointings. We cycled through the 27 pointings revisiting each of them every 800 seconds. Although this method does result in a small loss of uv-coverage for the longest baseline of interest (750 m), it produces an acceptable slew-time overhead of 10 per cent the total observing time. Observations of PKS B1934-638 were used for flux and bandpass calibrations. PKS 0332-403 was observed at 1.5 hr intervals (between on-source scans) for phase calibrations. The 64 MHz bandwidth, centred at 1396 MHz, was divided into 2048 channels providing a channel resolution of 31.25 kHz or 6.6 km s^{-1}.

The data were reduced and imaged using the MIRIAD software package (Sault, Teuben & Wright 1995). After flagging and calibration, the individual pointings were mosaicked to increase the signal-to-noise of the HI sources for better cleaning during the imaging process. We subtracted the radio continuum emission from the visibilities by fitting a polynomial to the line-free channels (using the UVLIN task in MIRIAD). For each pointing, the order of the polynomial was set to the lowest value which resulted in no residual continuum emission in the HI cube (typically 3). The naturally weighted HI sub-cube of the region around NGC 1427A has an 86 × 59 arcsec synthesized beam and an RMS noise of 3.1 mJy beam^{-1}. Fig. 1 shows the channel maps of the HI associated with NGC 1427A.

2.2 VST data

The optical observations of NGC 1427A are part of the Fornax Deep Survey (FDS) with OmegaCam on the VST (D'Abrusco et al. 2016; Iodice et al. 2016; Iodice et al. 2017; Venhola et al. 2017). OmegaCam has a 1 deg × 1 deg field of view and comprises an array of 8 × 4 CCDs, each with 2144 × 4200 pixels. OmegaCam's unbinned pixel size of 0.21 arcsec provides a well-sampled point spread function for the observations, which have an average full width at half maximum of ∼1 arcsec.

The currently available data were taken during visitor mode runs in 2013 November, 2014 November and 2015 November (ESO P92, P94 and P96, respectively). The VST mosaic of the inner two square degrees around the core of the Fornax cluster is presented by Iodice et al. (2016, see also https://www.eso.org/public/unitedkingdom/news/eso1612/?lang). In this paper, we used a small snapshot around NGC1427A taken from the whole mosaic in the four OmegaCam u', g', r' and i' bands, kindly provided by the FDS PIs. The observing strategy and data sets are described by Iodice et al. (2016).

The OmegaCam images presented in this paper were processed by using the AstroWISE pipeline, described in detailed by Venhola et al. (2017, see also McFarland et al. 2013). Instrumental corrections include the removal of bias and scattered light (background). The images have also been corrected for uneven illumination – by applying flat-field and illumination corrections – and calibrated to have a zero-point of 0. These observations have a 1σ photometric accuracy of 0.04, 0.02, 0.02 and 0.03 mag for u', g', r' and i', respectively (please refer to Venhola et al. 2017 for further details). Fig. 2 shows optical images of NGC 1427A in each band. In order to highlight the low surface brightness structures in these images, we performed a Gaussian smoothing with a radius of 10 pixels.

3 RESULTS

3.1 ATCA HI results

The ATCA observations provide sufficient resolution to resolve the extended HI structure of NGC 1427A (see Fig. 1). The properties of this galaxy as a whole (i.e. HI total flux, $F_{\rm H_I}$, central velocity, $v_{\rm H_I}$, and velocity widths, W_{50} and W_{20}, at 50 and 20 per cent of its respective peak flux), which are presented in Table 1, were measured using the HI source finding application SoFiA (Serra et al. 2015) and verified using manual measurement techniques (i.e. MBSPECT task in MIRIAD and the spectral profile plotting tool in CASA; McMullin et al. 2007). The difference in $F_{\rm H_I}$ obtained by each measurement method was added in quadrature to the noise in the cube resulting in an ∼10 per cent uncertainty. The global measurements of NGC

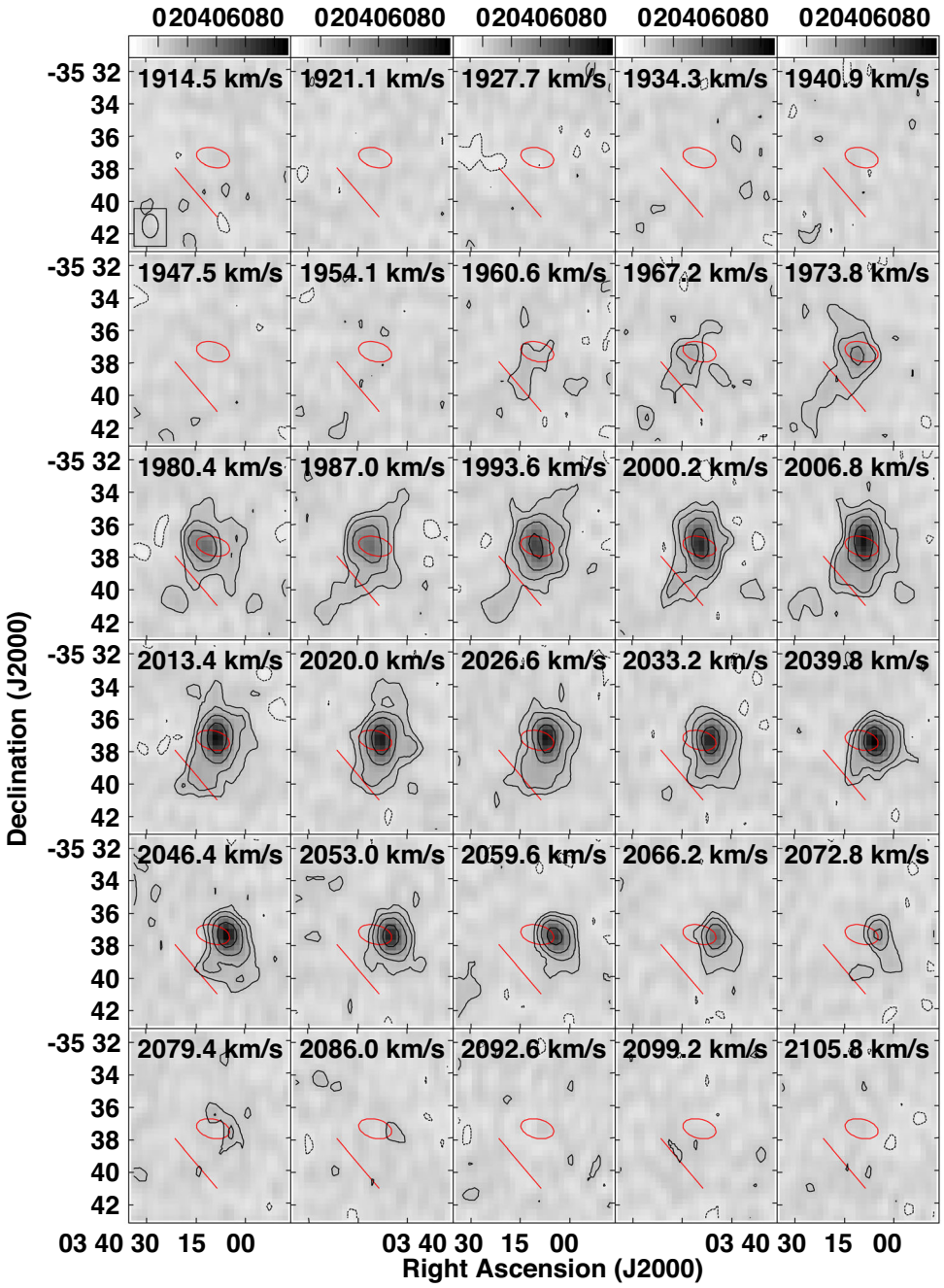

Figure 1. ATCA HI channel maps of NGC 1427A. The velocity of each channel is indicated at the top of each panel and the shape of synthesized beam is shown in the bottom left of the first panel. The HI intensity contours are at (−6, 6, 12, 24, 48) mJy beam^{-1}, with the negative contour indicated as the dashed line. The red ellipses represent the star-forming optical shape of the galaxy (see Fig. 2) and the red lines show the approximate boundary between HI in the main body of NGC 1427A and HI in the tail (see the text and Table 1 for further details).

1427A are consistent with values in the literature measured by Bureau et al. (1996) and Koribalski et al. (2004) using the single-dish Parkes radio telescope and presented in Table 2.

Fig. 3 shows the total intensity (i.e. moment-0) HI contours superimposed on a three-colour optical image of NGC 1427A, its moment-1 velocity map and the spatial location of this galaxy with respect to other Fornax cluster members. Within the ATCA cube, the only other HI features within an ∼1 deg (∼350 kpc) and ∼1000 km s^{-1} radius of NGC 1427A are ESO358-051, NGC 1437A and ESO 358-60, which were previously characterized by HIPASS, as well as a new HI detection, NGC 1437 (see Section 4 for further details about these neighbouring galaxies).

The HI channel maps in Fig. 1 show a bright central 'core' and up to three gaseous extensions. The most prominent extension – also clearly visible in Fig. 3b,c – is a newly resolved HI-rich tail extending towards the south-east of the optical centre of the galaxy. There also appears to be fainter HI extensions to the north and south-west of the core. Manually fitted ellipses were used to extract spectral profiles and derive the HI properties of the HI tail and the core region (the latter comprises all contiguous emission not included in

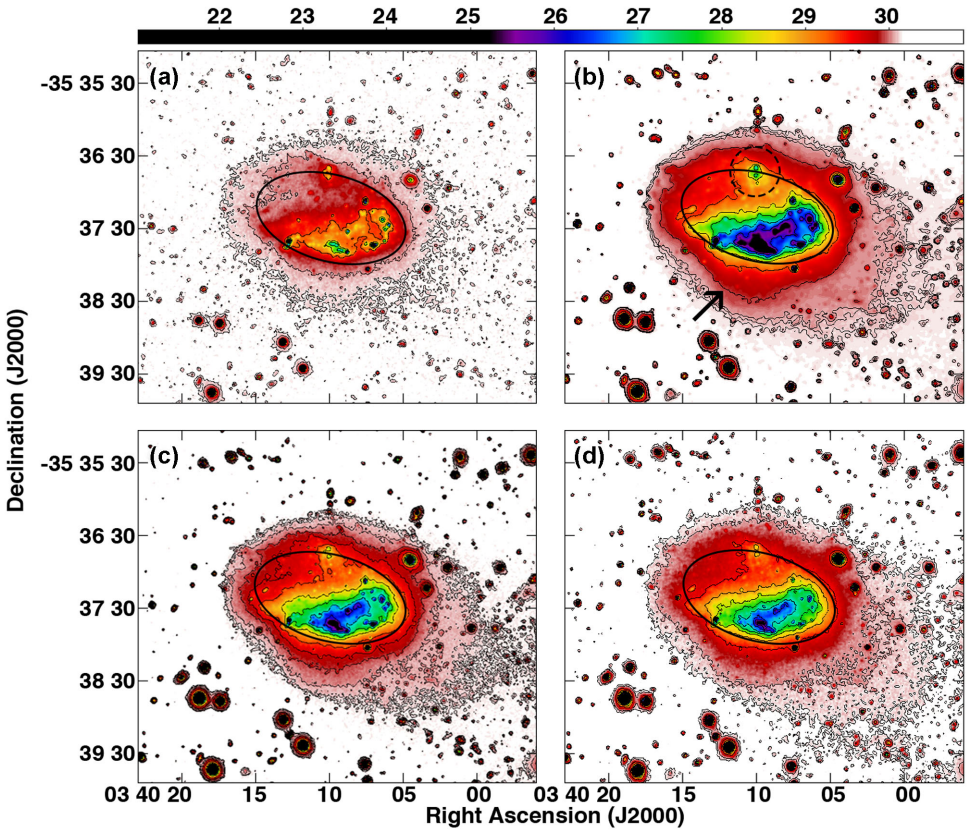

Figure 2. Smoothed VST images of NGC 1427A. The black ellipses are the same as the red ones shown in Fig. 1. (a) u'-band. (b) g'-band. The dashed circle indicates the northern stellar clump and the arrow points to a very faint stellar overdensity 'bump' (see the text for further details). (c) r'-band. (d) i'-band.

Table 1. HI properties of NGC 1427A, measured by ATCA. The uncertainties in $F_{\rm H_I}$ and $M_{\rm H_I}$ for the HI tail reflect the uncertainty in separating this component from the HI core region.

	NGC 1427A	HI tail	HI core region
Peak flux (Jy)	0.27 ± 0.02	0.038 ± 0.003	0.24 ± 0.02
$F_{\rm H_I}$ (Jy km s^{-1})	22 ± 2	2.1 ± 0.6	20 ± 2
$v_{\rm H_I}$ (km s^{-1})	2021 ± 3	1997 ± 3	2018 ± 3
W_{50} (km s^{-1})	80 ± 3	68 ± 3	77 ± 3
W_{20} (km s^{-1})	110 ± 3	76 ± 3	107 ± 3
$M_{\rm H_I}$ (10^9 $M_\odot$)	2.1 ± 0.2	0.20 ± 0.06	1.9 ± 0.2

Table 2. HI properties of NGC 1427A, measured by Parkes.

	Bureau et al. (1996)	Koribalski et al. (2004)
Peak flux (Jy)	–	0.261 ± 0.019
$F_{\rm H_I}$ (Jy km s^{-1})	23.1 ± 1.2	22.5 ± 3.0
$v_{\rm H_I}$ (km s^{-1})	2027.8 ± 0.8	2029 ± 4
W_{50} (km s^{-1})	83.4 ± 1.5	86
W_{20} (km s^{-1})	118.8 ± 1.0	119

the former). In Fig. 1, we indicate the approximate measurement boundary between the tail and core region. Shifting this line closer to the core ellipse can easily add up to 30 per cent more HI flux (and mass) to the tail. We describe the various components of NGC 1427A in the following subsections.

3.1.1 HI tail

The HI tail of NGC 1427A spans a velocity width of $W_{50} = 68 \pm 3$ km s^{-1} centred at 1997 km s^{-1}. With $F_{\rm H_I} = 2.1$ Jy km s^{-1}, this gaseous tail contains about 10 per cent of the HI mass ($M_{\rm H_I}$) of NGC 1427A. Considering that the radius of the central HI core of NGC 1427A (measured parallel to the tail) is ∼15 kpc, then the tail extends >20 kpc beyond the HI core (or >25 kpc beyond the stellar core). The alignment of this HI tail has significant implications on the direction of any ram pressure forces acting on NGC 1427A, which will be discussed in Section 4.

3.1.2 HI core region

The brightest HI contours in Fig. 1 coincide with the star-forming stellar core, indicated by the ellipses, of NGC 1427A. The distribution of most of the HI in the core is relatively symmetric and shows signs of rotation – with a clear velocity gradient – across the major axis of the disc (see also Fig. 3c). At the 2σ level, there is possibly an HI 'counter-tail' to the north of core at ∼1990 km s^{-1} and a faint HI cloud to south-west of the stellar core at ∼2003 km s^{-1}. These two marginally detected features appear to only span two velocity channels (∼10 km s^{-1}); nevertheless, their coincidence with other features warrants some mention. The possible counter-tail appears to be directly across from main HI tail at 1987–1994 km s^{-1} in Fig. 1, which is consistent with tidally formed features (see Toomre & Toomre 1972). Whereas, the faint HI cloud spatially coincides with some extended stellar emission (see Section 3.2.3).

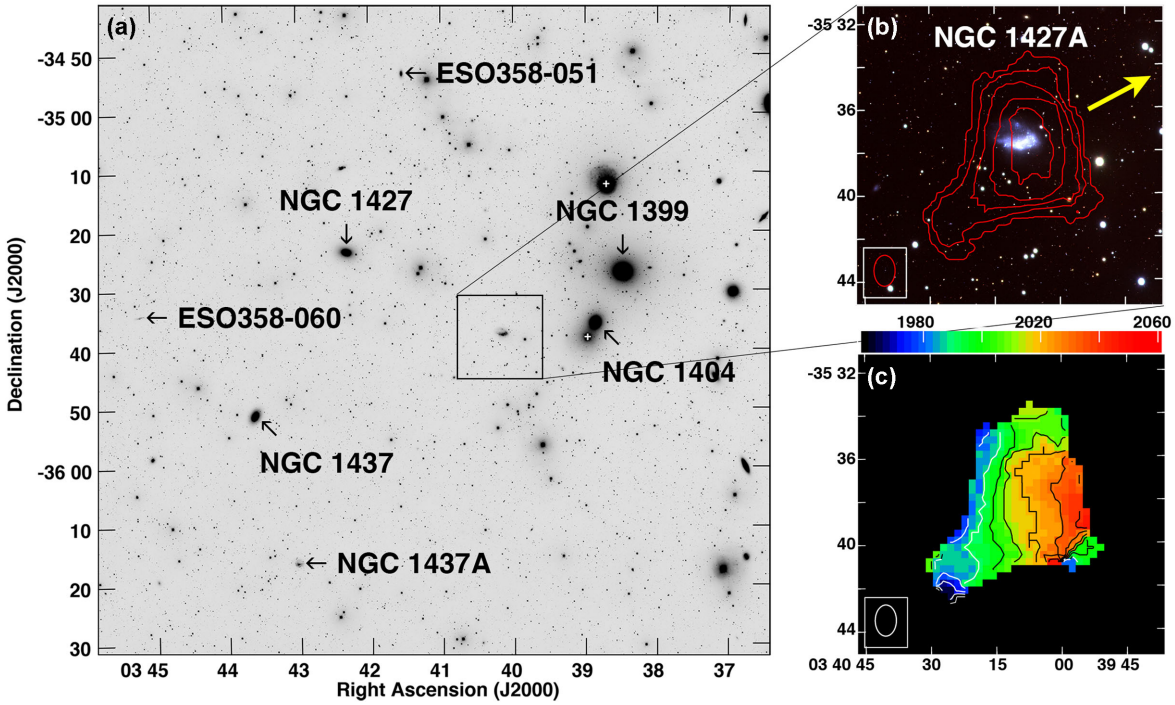

Figure 3. (a) VST r'-band image of central region of the Fornax cluster. Prominent cluster members are indicated by name and bright foreground stars are denoted by the white crosses. (b) ATCA total intensity HI (moment-0) contours from the SoFiA masked cube superimposed on a VST $g'r'i'$-band composite image of NGC 1427A. Contours are at (0.5, 1, 2, 5, 10) $\times$ 10^{20} atoms cm^{-2}. The yellow arrow points towards the central galaxy, NGC 1399. (c) ATCA HI velocity (moment-1) map. Contours are shown at 10 km s^{-1} increments.

Table 3. Global optical properties of NGC 1427A.

Property	Value	Units
R_{50}	34.2	arcsec
R_{90}	67.3	arcsec
$m_{r'}$	12.86	mag
$u' - r'$	1.27	mag
$g' - r'$	0.31	mag
$r' - i'$	0.20	mag
M_*	1.1×10^9	$M_\odot$

3.2 VST results

The global optical properties of this dIrr were measured from the original, unsmoothed VST images – using SExtractor (Bertin & Arnouts 1996), with the r'-band image as the reference for data extraction – and are presented in Table 3. R_{50} and R_{90} indicate the effective radii containing 50 and 90 per cent of the light, respectively. Each listed colour has been computed from the extracted apparent magnitudes (m_λ) in a Kron-like elliptical aperture for all bands. The stellar mass (M_*) of NGC 1427A has been estimated using the empirical relation calibrated by Taylor et al. (2011) and the assumed Fornax cluster distance, of 20 Mpc (Drinkwater et al. 2001a), to the source.

As seen in Fig. 2, NGC 1427A has an underlying elliptical shape visible in all four bands. The northern stellar clump is also detectable in the optical images. We find, for the first time, an extended region of low surface brightness stellar light south-west of the star-forming region. Furthermore, we also detect a stellar overdensity 'bump' extending towards the south, indicated in Fig. 2b. Fig. 4 is a $g' - r'$ colour image of NGC 1427A from VST observations which further highlights the irregular optical morphology of NGC 1427A. We describe the key stellar features in the following subsections.

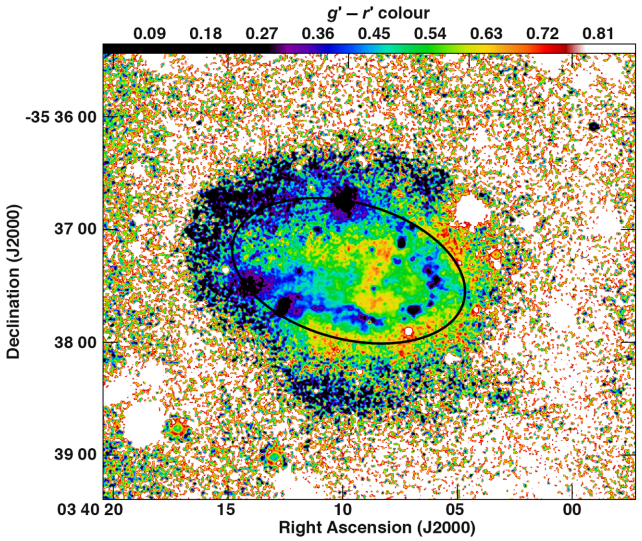

Figure 4. VST $g' - r'$ colour image of NGC 1427A. The black ellipse is the same as the ellipses shown in Figs 1 and 2.

3.2.1 *Stellar core*

The stellar core region is the bright central area of NGC 1427A, represented in Figs 1, 2 and 4 as a 125 $\times$ 70 arcsec ellipse with a position angle of 75 degree centred at 03h 40m 09.7s, $-35°$ 37′ 23″. As previously reported in the literature, there is active star formation along its south-west portion, which appears brightest in the g'-band.

Fig. 4 shows an irregular mixing of blue and red colours as there is a red arch external (and south-west) to the blue star-forming region and then a 'z' pattern of red stars near the centre. Most of the bright HI emission detected by ATCA coincides with this stellar core area (see Fig. 1).

3.2.2 Northern stellar clump

The northern stellar clump is located at 03h 40m 10s, −35° 36′ 45″ and, as shown in Fig. 4, is one of the bluest regions in NGC 1427A. Brightest in the g'-band, this clump is quite distinct from the other star-forming regions in the stellar core. The deep optical images are able to resolve some of the internal structure of this stellar clump and there appears to be hints of a slight arrow-shape pointing north with an extremely faint stellar trail to the south/south-west (see Fig. 2b), which is also detectable in the optical imaging by Hilker et al. (1997). Using *Hα* spectroscopy observations, Chaname et al. (2000) measure the heliocentric velocity of this feature to be ∼2029 km s^{-1}, well within the HI velocity range of NGC 1427A.

3.2.3 South-west extension

There is a substantial amount of diffuse light extending towards the south-west of NGC 1427A. This feature is ∼30 mag arcsec^{-2} and in the redder bands extends over half a disc-length away from the stellar core. There is a foreground star to the west of NGC 1427A (located at 03h 41m 45s, −35° 28′ 57″), however, the reflection halo of that star appears to have negligible contribution to the stellar light in the south-west extension. This extension is located south-west of the bright star-forming region in the stellar core. Such extended emission would not be expected if ram pressure forces impacted that side of the galaxy, which will be further discussed in Section 4.

3.2.4 Southern bump

The deep VST optical images also reveal a stellar overdensity bump extending towards the south, indicated by the arrow in Fig. 2b. This bump is less extended but somewhat brighter in the g' and r' bands than the south-west extension and is similar in colour as the north-east portion of NGC 1427A (see Fig. 4). The southern bump appears to spatially coincide with the base of the HI tail of NGC 1427A. In fact, while the VST images are able to detect fairly diffuse and extended features, there appears to be no substantial stellar counterpart for the HI tail of NGC 1427A.

4 DISCUSSION

NGC 1427A has long been regarded as a good candidate for studying the effects of ram pressure stripping in the Fornax cluster. A number of previous studies concluded that the disturbed optical appearance of NGC 1427A is due to its passage through and interaction with the dense ICM (e.g. Chaname et al. 2000; Mora et al. 2015). Our resolved HI observations and deep optical imaging of NGC 1427A allow us to study the distribution of gas and stars in the outskirts of this galaxy and constrain the processes affecting its irregular morphology.

4.1 Is NGC 1427A located within the Fornax Cluster?

Definitive distance measurements of NGC 1427A and its position within the Fornax cluster could determine which dynamical processes are affecting this object. If the galaxy is located in the outskirts, away from the cluster potential, then tidal interactions would clearly give rise to its irregular optical morphology. If it is deep within the cluster, then ram pressure would be the cause of this dIrr's arrow-shaped appearance.

Optical spectroscopy by Drinkwater et al. (2001a) shows that a significant number of star-forming dwarf galaxies are infalling on to the Fornax cluster. Based on its position and recessional velocity, NGC 1427A could be part of this infalling population. A comparison between the turnovers of the globular cluster luminosity function of NGC 1427A and NGC 1399 (the central cluster galaxy) places the former 3.2 Mpc ± 2.5 Mpc (statistic) ± 1.6 Mpc (systematic) in front of the latter (Georgiev et al. 2006). NGC 1427A might therefore be several Mpc away from the cluster centre, where ram pressure would be ineffective (Vollmer et al. 2001). However, the large statistic and systematic error on this estimate makes it difficult to reach a definitive verdict. There is still the possibility that NGC 1427A is located within a region where interactions with the ICM can be a factor.

The most prominent spatially (in projection) and spectrally close neighbour to NGC 1427A is NGC 1404, a giant elliptical with an X-ray envelope that is currently being distorted by its infall towards NGC 1399 (Jones et al. 1997). Distance measurements using a wide variety of indicators suggest that NGC 1404 is either ∼1 Mpc behind (e.g. Ferrarese et al. 2000; Tonry et al. 2001; Jensen et al. 2003) or over 2 Mpc in front of (e.g. Liu, Graham & Charlot 2002; Tully et al. 2013) other major cluster members. Considering the uncertainty on the only independent distance measurement for NGC 1427A (i.e. Georgiev et al. 2006) and the variance in methods used to estimate distances to different types of galaxies, it is difficult to analyse any relationship (or lack thereof) between NGC 1427A and NGC 1404.

Overall, due to the uncertainty in previously obtained distance measurements as well as the high velocity dispersion in the cluster environment that prohibits using radial velocity measurements as a proxy for distance, it is quite challenging to determine whether NGC 1427A is located within the Fornax cluster. Accordingly, we discuss and compare our observed results in the context of ram pressure, tidal interactions and a combination of these two processes in the following sections.

4.2 Ram pressure hypothesis

Under the ram pressure hypothesis and given the location of its younger blue stars (as shown in Fig. 2a), NGC 1427A would be moving in a south-west direction within the cluster. The ram pressure wind would therefore be acting towards the north-east. Ram pressure is particularly effective at displacing gas at the outskirts of a galaxy relative to its stellar body (e.g. Chung et al. 2009; Kenney et al. 2014; Kenney, Abramson & Bravo-Alfaro 2015; Abramson et al. 2016). For example, ESO137-001 is an infalling galaxy in the Norma cluster that has an extended gaseous tail and a modestly intact interior stellar region (Sun et al. 2010).

If ram pressure is acting on NGC 1427A, any HI at large galactic radii should form a tail extending towards the north-east, relative to the centre of the galaxy. However, our detection of a >20 kpc long HI tail pointing perpendicular to this direction (i.e. towards the south-east) contradicts the ram pressure hypothesis. Additionally, the diffuse stellar extension as well as the faint HI feature extending towards the south-west of the galaxy greatly opposes the expected ram pressure induced compression along that region.

Jones et al. (1997) and Paolillo et al. (2002) do show that the X-ray envelope of NGC 1399 extends out, in projection, to NGC 1427A. However, given the current uncertainty on the position of NGC 1427A relative to the Fornax cluster volume, this dIrr is not necessarily immersed within this hot gas and the evidence for the interaction between this galaxy and the ICM remains poor. We note that NGC 1427A appears to be an X-ray source in those images, which could be interpreted as another result against ram pressure. Presumably, if ram pressure was occurring, it would have removed the hot X-ray halo prior to stripping the cold HI disc of this galaxy.

4.3 Tidal interactions

If the arrow-shaped appearance of NGC 1427A is not the result of ram pressure, then the other obvious explanation would be that tidal interactions have caused the recent burst in star formation. The most conspicuous interloper would be the northern stellar clump of NGC 1427A. Previous work ruled out this stellar clump as an intruder based on kinematical alignment (Chaname et al. 2000); nevertheless, it has been shown that some HI satellites, which are accreted by larger galaxies, join the rotation of the parent's disc (Sancisi 2008). This northern clump is also very blue, even compared to the other star-forming regions, which could indicate that it is still actively interacting with NGC 1427A.

The overall stellar component of NGC 1427A appears to be redder at larger radii and extends well beyond the galaxy's star-forming region, implying that star formation is being triggered within the disc. Additionally, the irregular mixing of colours in the stellar core possibly indicates the presence of two objects in the process of merging. Depending on the initial parameters of the interaction, it is quite likely that the northern stellar clump started as a separate object and is the main contributor to the optical appearance of NGC 1427A.

Alternatively, we explore the possibility that the tidal disturbance was triggered by a recent fly-by of another galaxy in the cluster. The nearest HIPASS detected HI-rich galaxies to NGC 1427A are ESO358-051 (HIPASS J0341–34; 03h 41m 06s, −35° 56′ 02″; $F_{\rm H_I}$ = 4.84 Jy km s^{-1}, $v_{\rm H_I}$ = 1734 km s^{-1}), ESO358-060 (HIPASS J0345–35; 03h 45m 12s, −35° 34′ 07″; $F_{\rm H_I}$ = 11.34 Jy km s^{-1}, $v_{\rm H_I}$ = 803 km s^{-1}) and NGC 1437A (HIPASS J0342–36; 03h 42m 52s, −35° 17′ 26″; $F_{\rm H_I}$ = 7.61 Jy km s^{-1}, $v_{\rm H_I}$ = 895 km s^{-1}; Waugh et al. 2002). The ATCA data for these galaxies detect comparable amounts of HI to the values measured from HIPASS.

ESO358-051 is located >200 kpc and >200 km s^{-1} from NGC 1427A, while ESO358-060 is ∼350 kpc and >1200 km s^{-1} away. Both these galaxies show no clear morphological signs of being involved in a recent fly-by interaction. Whereas, NGC 1437A has a similar arrow-shaped optical appearance as NGC 1427A and seems to be travelling in a south-east direction (based on the location of its own star-forming region) which is parallel with the orientation of NGC 1427A's HI tail. NGC 1437A has about one third the HI mass as NGC 1427A and the velocity difference between these dIrrs is ∼1150 km s^{-1}, which is three times higher than the velocity dispersion of the Fornax cluster. However, if these two galaxies experienced a previous fly-by interaction and their velocity difference translates into their movement away from one another, then it would take a few hundred Myr to move 300 kpc (i.e. their projected separation distance) apart, which is considerably longer than the recent starburst episode occurring 4 Myr ago as measured by Mora et al. (2015). The ATCA observations also detect unresolved HI centred on NGC 1437, however, this galaxy has a fairly regular optical appearance that, similar to the previously discussed ESO galaxies, has no indication of recent tidal interactions.

Overall, the ATCA data rule out signs of tidal disturbances with a projected linear size of ∼6 kpc (at a distance of 20 Mpc) down to a column density of 3 × 10^{19} atoms cm^{-2}; however, with a 1.4 × 1 arcmin beam, several HI detections are only marginally resolved. In the currently available catalogues of Fornax region galaxies with known redshifts (i.e. Drinkwater et al. 2001b; Morris et al. 2007; Blakeslee et al. 2009), there is also no clearly apparent external tidal disturber of NGC 1427A. The deep VST observations do detect a multitude of low surface brightness galaxies, two of which are – in projection – located near the tip of HI tail (Venhola et al. 2017); however, without reliable distance measurements it is difficult to establish any physical association.

4.4 Tidal interactions + ram pressure

We have effectively ruled out ram pressure acting from the south-west as the cause of the arrow-shaped optical morphology of NGC 1427A. It seems most-likely that the northern stellar clump was once a separate object that is now merging with the main body of NGC 1427A. This tidal interaction could also be responsible for the formation of the newly detected HI tail. Although tidal tails typically form in pairs and generally have associated stellar components (Toomre & Toomre 1972; Kaviraj et al. 2012), it is possible to have a single tail and to form tidal debris with no detectable optical counterpart (e.g. Chung et al. 2007; Lee-Waddell et al. 2014). We note that there is a hint of a counter-tail extending towards the north of the HI core, however, this feature is only marginally detected (see Section 3.1.2).

The HI tail could have formed as it is currently seen or, dependent on the location of NGC 1427A within the Fornax cluster, ram pressure could have a role in shaping this tail. Tidal interactions could have initially expelled HI to the galaxy's outskirts. Subsequently, ram pressure could have swept together any tidally formed HI tails creating a single trailing tail (see Chung et al. 2007). This sequence of events would be consistent with the presence of the southern stellar bump, which spatially coincides with the base of the HI tail. Starting from such a bump, the HI could have been moved to larger radii by ram pressure, leaving the stellar body relatively intact. In this case, the implied movement of NGC 1427A within the cluster is towards the north-west, in the direction of the cluster centre. Such motion would indicate a more radial orbit of NGC 1427A within Fornax than previously suggested by the literature.

5 CONCLUSIONS

We have detected an HI tail and extended stellar emission that sheds new light on the recent history of NGC 1427A. The spatial position and distance of this dIrr indicate a possible association with the Fornax cluster (Drinkwater et al. 2001b), however, without accurate distance measurements, it is difficult to determine its exact location relative to the cluster and its current direction of travel. Our new data rule out a ram pressure origin for the arrow-shaped optical appearance of NGC 1427A. There is significant evidence that suggests a previous tidal interaction (with another Fornax cluster member) or a recent merging event has occurred to induce the recent starburst episode. The irregularly mixed optical colours in the core of NGC 1427A and its distinct northern stellar clump favour the latter scenario.

This same interaction event could have formed the HI tail *in situ*. Alternatively, a combination of tidal and ram pressure forces could

have swept any tidally formed tails into the currently detectable HI tail, thereby indicating that NGC 1427A is travelling in a north-west direction, towards the cluster centre. Regardless of the exact combination of mechanisms that are affecting NGC 1427A, our new observations do make it apparent that tidal interactions are predominantly at play in this system.

ACKNOWLEDGEMENTS

We thank the anonymous reviewer for his/her detailed suggestions and insightful comments to improve the clarity of this paper. The Australia Telescope Compact Array is part of the Australia Telescope National Facility which is funded by the Australian Government for operation as a national facility managed by CSIRO. This project has received funding from the European Research Council (ERC) under the European Union's Horizon 2020 research and innovation programme (grant agreement no. 679627; project name FORNAX). BC is the recipient of an Australian Research Council Future Fellowship (FT120100660).

REFERENCES

Abramson A., Kenney J., Crowl H., Tal T., 2016, AJ, 152, 32
Bertin E., Arnouts S., 1996, A&AS, 117, 393
Blakeslee J. P. et al., 2009, ApJ, 694, 556
Bournaud F. et al., 2007, Science, 316, 1166
Bureau M, Mould J. R., Staveley-Smith L., 1996, ApJ, 463, 60
Cellone S. A., Forte J. C., 1997, AJ, 113, 1239
Chaname J., Infante L., Reisenegger A., 2000, ApJ, 530, 96
Chung A., van Gorkom J. H., Kenney J., Vollmer B., 2007, ApJ, 659, 115
Chung A., van Gorkom J. H., Kenney J., Crowl H., Vollmer B., 2009, AJ, 138, 1741
D'Abrusco R. et al., 2016, ApJ, 819, 31
Drinkwater M. J., Gregg M. D., Colless M., 2001a, ApJ, 548, L139
Drinkwater M. J., Gregg M. D., Holman B. A., Brown M. J. I., 2001b, MNRAS, 326, 1076
Ferrarese L. et al., 2000, ApJ, 529, 745
Georgiev I. Y., Hilker M., Puzia T. H., Chanamé J., Mieske S., Goudfrooij P., Reisenegger A., Infante L., 2006, A&A, 452, 141
Gunn J. E., Gott J. R., 1972, ApJ, 176, 1
Hilker M., Bomans D. J., Infante L., Kissler-Patig M., 1997, A&A, 327, 562
Iodice E. et al., 2016, ApJ, 820, 42
Iodice E. et al., 2017, ApJ, 839, 21
Jensen J. B., Tonry J. L., Barris B. J., Thompson R. I., Liu M. C., Rieke M. J., Ajhar E. A., Blakeslee J. P., 2003, ApJ, 583, 712
Jones C., Stern C., Forman W., Breen J., David L., Tucker W., 1997, ApJ, 482, 143
Kaviraj S., Darg D., Lintott C., Schawinski K., Silk J., 2012, MNRAS, 419, 70
Kenney J. D. P., Geha M., Jachym P., Crowl H. H., Dague W., Chung A., van Gorkom J., Vollmer B., 2014, ApJ, 780, 119
Kenney J. D. P., Abramson A., Bravo-Alfaro H., 2015, AJ, 150, 59
Koribalski B. S. et al., 2004, AJ, 128, 16
Lee-Waddell K. et al., 2014, MNRAS, 443, 3601
Liu M., Graham J., Charlot S., 2002, ApJ, 564, 216
McFarland J. P., Verdoes-Kleijn G., Sikkema G., Helmich E. M., Boxhoorn D. R., Valentijn E. A., 2013, ExA, 35, 45
McMullin J., Waters B., Schiebel D., Young W., Golap K., 2007, ASPC, 376, 127
Mihos J. C., Harding P., Feldmeier J., Morrison H., 2005, ApJ, 631, 41
Mora M. D., Chaname J., Puzia T. H., 2015, AJ, 150, 93
Morris R. A. H., Phillipps S., Jones J. B., Drinkwater M. J., Gregg M. D., Couch W. J., Parker Q. A., Smith R. M., 2007 A&A, 476, 59
Paolillo M., Fabbiano G., Peres G., Kim D.-W., 2002, ApJ, 565, 883
Sancisi R., Fraternali F., Oosterloo T., van der Hulst T., 2008, A&AR, 15, 189
Sault R. J., Teuben P. J., Wright M. C. H., 1995, in Shaw R. A., Payne H. E., Hayes J. J. E., eds, ASP Conf. Ser. Vol. 77, Astronomical Data Analysis Software and Systems IV. Astron. Soc. Pac., San Francisco, p. 433
Serra P., 2015, MNRAS, 448, 1922
Sun M., Donahue M., Roediger E., Nulsen P. E. J., Voit G. M., Sarazin C., Forman W., Jones C., 2010, ApJ, 708, 946
Taylor E. et al., 2011, MNRAS, 418, 1587
Toloba E., 2014, ApJ, 783, 120
Tonry J. L., Dressler A., Blakeslee J. P., Ajhar E. A., Fletcher A. B., Luppino G. A., Metzger M. R., Moore C. B., 2001, ApJ, 546, 681
Toomre A., Toomre J., 1972, ApJ, 178, 623
Tully R. et al., 2013, AJ, 146, 86
Venhola A. et al., 2017, A&A, in press
Vollmer B., Cayatte V., Balkowski C., Duschl W. J., 2001, ApJ, 561, 708
Waugh M. et al., 2002, MNRAS, 337, 641

This paper has been typeset from a TEX/LATEX file prepared by the author.